

Data processing workflow for time of flight polarized neutrons inelastic measurements

Andrei T Savici¹, Igor A Zaliznyak², V Ovidiu Garlea¹ and Barry Winn¹

¹NScD, Oak Ridge National Laboratory, Oak Ridge, TN., USA

²CMPMSD, Brookhaven National Laboratory, Upton, NY, USA

E-mail: saviciat@ornl.gov

Abstract. We discuss the data processing workflow for polarized neutron scattering measurements performed at HYSPEC [1] spectrometer at the Spallation Neutron Source, Oak Ridge National Laboratory. The effects of the focusing Heusler crystal polarizer and the wide-angle supermirror transmission polarization analyzer are added to the data processing flow of the non-polarized case. The implementation is done using the Mantid [2] software package.

1. Introduction

The polarized neutron scattering has proved to be an invaluable tool for distinguishing between nuclear and magnetic cross-sections. Recent advances in instrumentation allow scattering measurements using large area, position-sensitive detectors. Such experiments are routine for unpolarized neutrons. However, polarization analysis on wide angle detectors pose some challenges, which we are discussing in this paper.

Traditionally, polarized inelastic neutron investigations of the sample dynamical properties were carried out using triple axis spectrometers [3]. A schematic representation of such an instrument is shown in Figure 1. A monochromatic neutron beam is produced when neutrons from the source (moderator) are Bragg-reflected by the monochromator crystal. To produce a polarized neutron beam, one can use a monochromator made of Heusler crystals, magnetized so that they only reflect one neutron spin state, or insert a polarized ³He cell, which only transmits one spin state along the monochromator to sample flight path. The incident beam polarization can be rotated using an adiabatic guide field, and inverted with respect to this direction using a Mezei flipper. From the scattered beam, an analyzer crystal selects only neutrons with a certain final energy. The post-sample instrument components can select a particular neutron polarization, using a setup similar to the one described for the incident beam. The analysis workflow for polarized experiments is very similar to unpolarized experiments. In the case

¹ This manuscript has been authored by UT-Battelle, LLC under Contract No. DE-AC05-00OR22725 with the U.S. Department of Energy. The United States Government retains and the publisher, by accepting the article for publication, acknowledges that the United States Government retains a non-exclusive, paid-up, irrevocable, worldwide license to publish or reproduce the published form of this manuscript, or allow others to do so, for United States Government purposes. The Department of Energy will provide public access to these results of federally sponsored research in accordance with the DOE Public Access Plan (<http://energy.gov/downloads/doe-public-access-plan>).



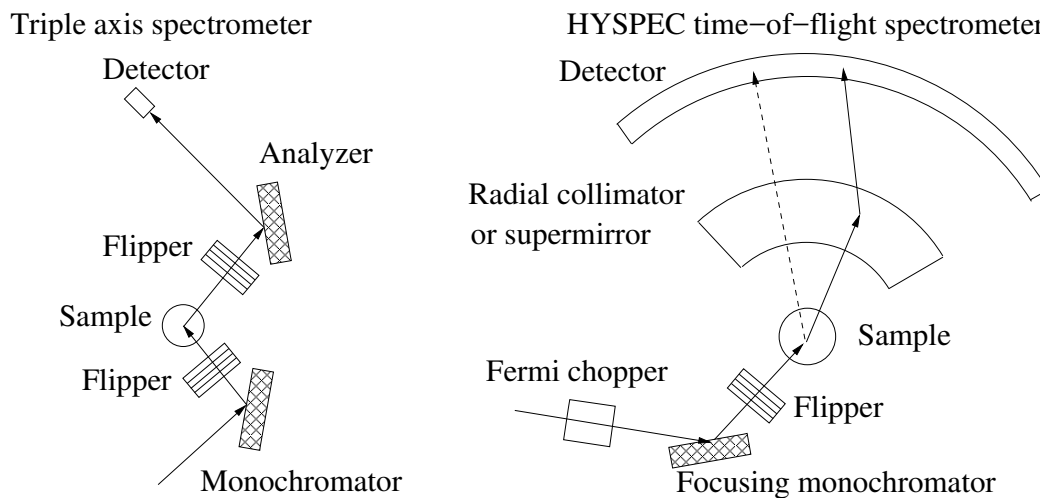


Figure 1. Comparison of the polarized neutron scattering setup for a triple axis spectrometer and a time-of-flight direct geometry spectrometer. For the HYSPEC spectrometer, a radial collimator, or a supermirror analyzer can be inserted in the scattered neutron path between the sample and the detector. Neutrons are not deflected in the radial collimator (dashed path), but their trajectory is changed for the supermirror analyzer case (solid path).

that Heusler crystals are used, the scattering angle and reflectivity are different from the case of non-polarized setup, but, with a single detector, calibrating the polarization efficiency is straightforward.

The HYSPEC spectrometer [1] at the Spallation Neutron Source, Oak Ridge National Laboratory has recently started measurements in the fully polarized mode. The incident neutron beam is monochromated by a short-blade (“rotating collimator”) Fermi chopper. The beam is then reflected by a vertically focusing crystal array, thus increasing the flux on the sample at the expense of vertical resolution. For unpolarized experiments, the focusing array made of pyrolytic graphite (PG) is used. For polarized measurements, a Heusler crystals array is used. In unpolarized or half-polarized measurements, a radial collimator, which defines the scattering volume viewed by detectors is placed immediately after the sample, at a fixed position (not oscillating), well in front of the detector array. For fully polarized experiments, the radial collimator is replaced with the similarly sized, 60°-wide-angle supermirror array, which selects a single neutron polarization. The scattered neutrons that passed through a collimator, or a supermirror, are detected by the two-dimensional (2D) position sensitive array of detectors (160 vertical tubes, 1.2 m long, 128 pixels each) covering ≈ 0.27 sR ($w \times h = 60^\circ \times 15^\circ$). A schematics of the HYSPEC setup is shown in Figure 1. Details of the geometry of the instrument can be found in a complementary paper in the same conference proceedings [4]. Similarly to the other SNS instruments, the data on HYSPEC is collected in the event mode, where information about each detected scattered neutron is individually stored.

The principal advantage of the time-of-flight spectrometers for the inelastic neutron scattering measurements is in the capability of surveying large volumes of the reciprocal space at a time. In the current polarized setup this requires properly accounting for the transmission probability through the instrument, which is heavily dependent on the neutron’s path and energy.

2. Characterization of the polarizing components

In a polarized neutron scattering experiment, it is important to maximize both the polarization efficiency and the transmission through the instrument, which both need to be assessed experimentally. In the HYSPEC setup, characterizations of different components of the instrument were performed using an isotropic incoherent scatterer, made of TiZr alloy. In order to characterize the dependence of the transmission on the horizontal scattering angle, one can group all pixels in a vertical tube, to get better statistics. The grouping occurs after conversion of data from time-of-flight to energy transfer, so the different secondary flight paths are taken into account. The effect of this procedure on the vertical momentum transfer is comparable in magnitude with the effect of the focussing monochromator (the size of Bragg peaks on the detector array is about one third of the tube length in vertical direction).

Measurements of the reflectivity of the Heusler monochromator (not shown in this paper) exhibit the same intensity pattern in the detector as for the pyrolytic graphite monochromator (no tube to tube variation). The reflectivity ratio is slightly incident energy dependent, and independent of the energy resolution of the incident beam (Fermi chopper frequency).

For the comparative evaluation of the transmission through the supermirror array and the radial collimator, we measured the same TiZr alloy sample in both cases using the PG monochromator (higher flux). As seen in Figure 2 (top left panel), the scattering intensity from

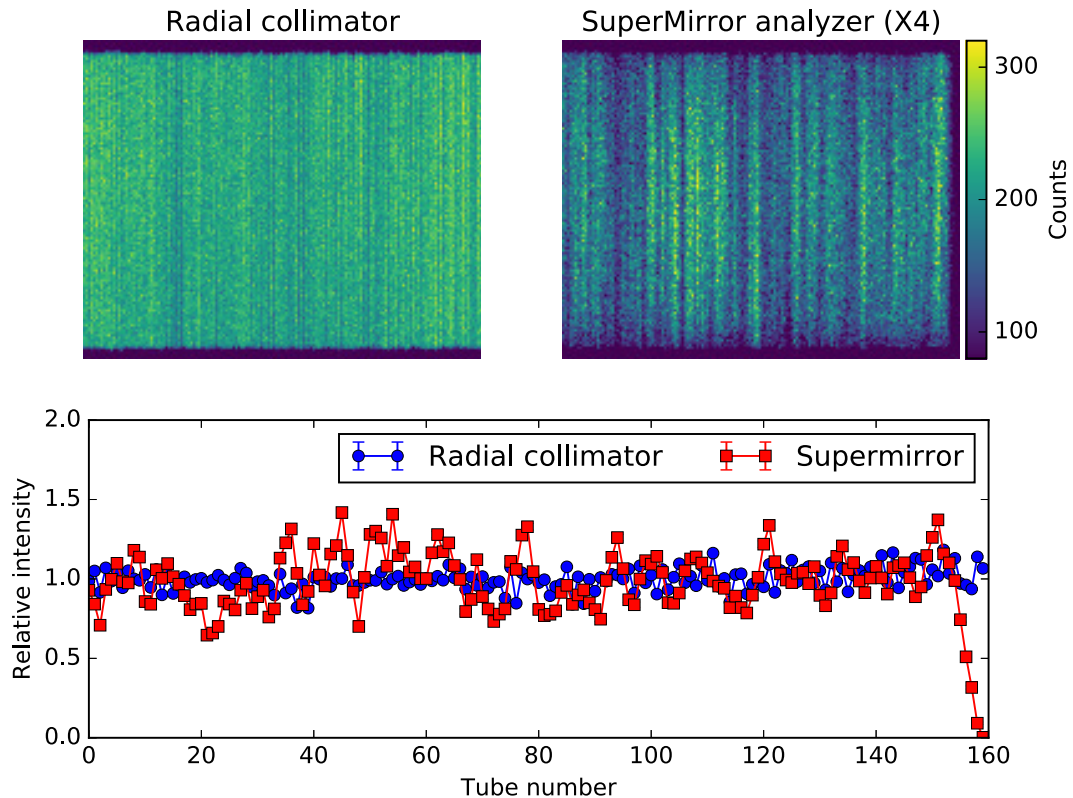


Figure 2. Position dependent transmission of the radial collimator and the supermirror analyzer, as seen in the corresponding images of the HYSPEC detectors, measured with 3.8 meV incident energy. The radial collimator has a uniform transmission (top left). The supermirror analyzer intensity (top right - multiplied by 4 to be on the same scale) shows angle-dependent inhomogeneity. The relative intensity variation of the elastic line integrated in energy and over the tube length is shown at the bottom.

such an incoherent source measured with the radial collimator after sample is relatively flat. In the case of the supermirror polarizer, the transmission is markedly inhomogeneous (top right panel). Notably, the last few detector tubes on the right side are not illuminated at all. The reason for this is the deflection of the beam by the supermirror analyzer. While the geometry of the analyzer-detector channels on HYSPEC is similar to that on the D7 instrument at ILL [5], their angular positions are referenced by the scattering angle at the entrance to the analyzer channel (neutronic positions). These are different from the corresponding angles at the exit of the analyzer, while the angles of the detector pixels, which are about 4 m away from the analyzer, are parameterized by their physical positions and correspond to the angles at the analyzer entrance, as in the case of the unpolarized neutrons. To exclude colormap bias when looking at the angular dependent intensity pattern, we integrated the elastic scattering in each tube. The relative intensity of each tube, with respect to the average for the configuration, is shown in the bottom panel of Figure 2. For the supermirror analyzer only the first 155 tubes were considered in the calculation of the average. We found that the intensity pattern on the detector for the supermirror array transmission is sample position dependent. This is not surprising since the small angular acceptance of a single analyzer channel, combined with the short sample to analyzer distance, yield a small horizontal acceptance interval for each individual channel. To account for this effect, at the end of each experiment we measure the incoherent scattering from a Vanadium reference placed at the sample position. The dimensions of the Vanadium reference are compatible with the acceptance width of the analyzer system (6.3 mm diameter).

For the transmission measurements, we masked (in software) the top and the bottom 8 pixels of the tubes and the tubes shadowed by the beam deflection in the analyzer. The neutron count integrated over thus defined PSD area for the elastic scattering at different energies is shown in Figure 3. The measured TOF data was transformed to the energy transfer, and a Gaussian fit of the elastic line was used for evaluating the intensity on top of a linear background. The total count in the peak was corrected for the energy dependent detector efficiency and normalized to the same proton charge. Thus obtained intensities in the left panel of Figure 3 contain the energy dependent incident flux. In order to obtain the transmission through the supermirror array, we divide the corresponding measured intensity with the one for the radial collimator case, and multiply by 2 to account for the relative fraction of neutrons with one spin polarization: both polarization are transmitted by the radial collimator, but only one by the supermirror array. For the ideal polarizer, one would expect a transmission $T = 1$. The resulting dependence of the polarizer transmission on the neutron energy (E_F) is shown in Figure 3. We found that we can empirically describe this dependence as an exponential, $T \sim e^{-E_F/E_0}$.

Since the transmission through the supermirror at each given incident energy is position- (angle-)dependent (as seen in Figure 2), and the overall average transmission varies with the energy, we checked if the energy dependence of the transmission is the same for each tube, or not. The results are shown in Figure 4. The transmission for each tube is shown on the left side. Each curve has been fitted with the same exponential dependence as the overall transmission,

$$T = T_0 e^{-E_F/E_0} . \quad (1)$$

The scatter plot of the T_0 and E_0 parameters against each other is shown in the right panel of Fig. 4. We found that the points cluster around the values obtained by fitting the intensity integrated over all detectors. Future instrument upgrades, which will allow fine-tuning the supermirror alignment could perhaps narrow the spread of the E_0 parameter, reducing the regular tube-dependent variation of the transmission at a given energy. Finally, the present procedure only accounts for the energy dependence of the neutron beam deflection in the supermirror by virtue of the energy-dependent transmission calibration. While this introduces a systematic error in the energy-wave vector calculation, this error is small, while implementing in Mantid [2] a procedure which would account for both the varying transmission and the varying

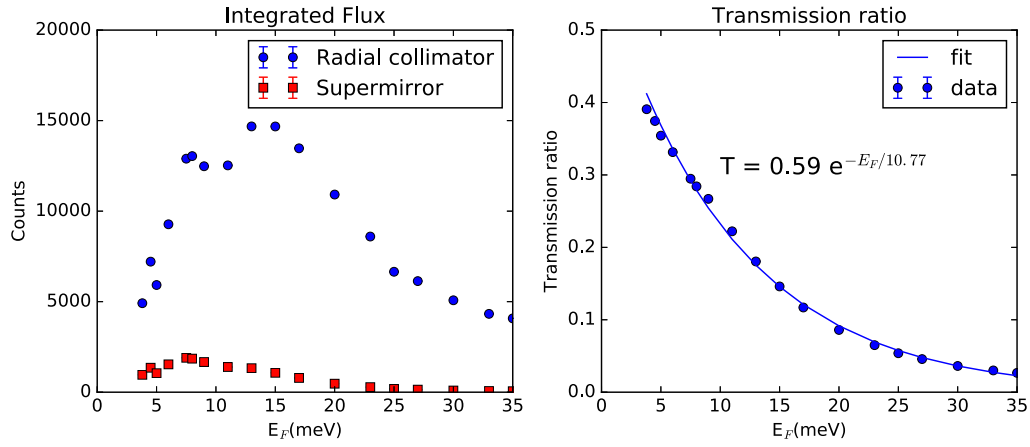


Figure 3. Energy dependent flux at the detector measured with radial collimator or supermirror after the sample. (left) absolute values (right) transmission through the supermirror measured as a ratio of the fluxes through the supermirror and the radial collimator, multiplied by 2.

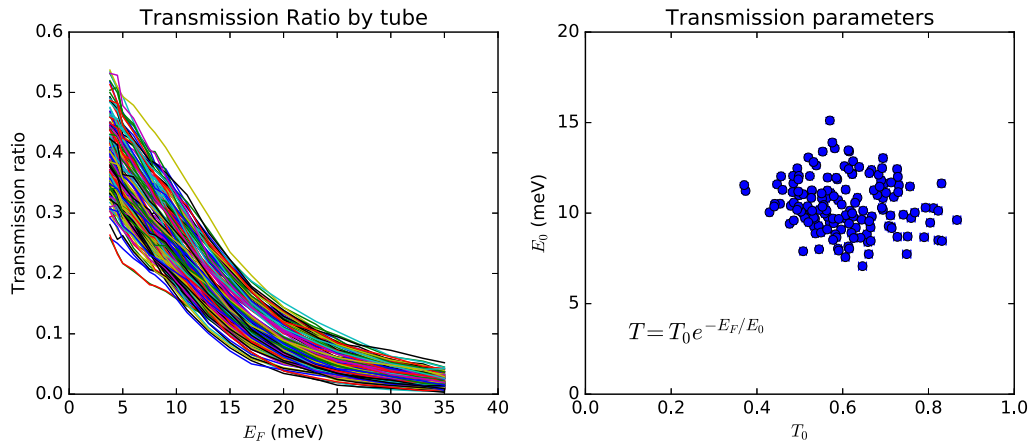


Figure 4. Energy dependent transmission for detector tubes. (left) Raw data showing an exponential dependence (right) Fit parameters (see text for details)

beam deflection is challenging. We nevertheless plan such work for the future.

The last step in characterization of the supermirror array is a measurement of the polarization efficiency. Results are shown in Figure 5. The Heusler alloy monochromator has been used to polarize the incident beam. For the isotopic incoherent scattering, like in the case of the TiZr alloy used for this measurement, we expect to have intensity only in the non spin flip channel. The flipping ratio is then defined as the ratio of scattered intensities in the non spin flip and the spin flip channels, or with the flipper ON and the flipper OFF, correspondingly, in the case of the HYSPEC setup,

$$F = \frac{I^{++}}{I^{+-}} = \frac{I^{ON}}{I^{OFF}}. \quad (2)$$

The analysis was performed on each individual tube by fitting the corresponding elastic line

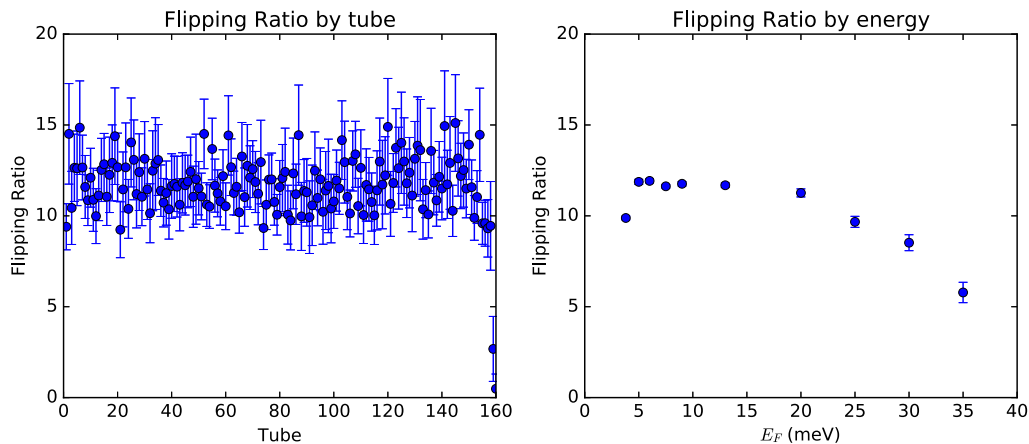


Figure 5. Measurement of system-wide flipping ratio. (left) At constant energy (13 meV) the flipping ratio is independent of the detector tube. (right) Energy dependence integrated over the whole instrument

intensities to Gaussian profiles on top of a linear background. We observe no angular dependence of the flipping ratio in the detectors that are not shadowed by beam deflection in the supermirror analyzer. This is in contrast to the result for the angle-dependent transmission seen in Figures 2 and 4. The right panel of Figure 5 presents the energy dependence of the flipping ratio obtained by adding counts from all detectors. It is relatively constant up to about 20 meV, with a gradual decrease at higher energies. The reason for the lower flipping ratio measured at incident energy of 3.8 meV remains unclear.

3. Data reduction workflow

Data reduction is the process of transforming the time-of-flight event data into quantities that have some physical meaning in the sample parameter space, independent of the measurement details. For the case of HYSPEC, the original data is stored as a collection of time of flights when neutron events were collected. The final outcome of the reduction, the scattering cross section, or the cumulative dynamical structure factor (i. e. the sum of the structure factors of all scatterers in the neutron beam), is stored as a histogram in terms of momentum and energy transfer. The workflow that we describe in this paper is implemented using the Mantid [2] software suite. It tries to follow, as much as possible, the workflow for unpolarized experiments. If not explicitly marked as polarized only steps, individual items in the workflow are common to both polarized and unpolarized experiments.

- (1) Pre-process the incoherent scattering data from a Vanadium, or a TiZr alloy sample: the angle- and energy-dependent transmission and the flipping ratio are stored for later use. This step is not performed for unpolarized neutron case, where the transmission is uniform.
- (2) Load data.
- (3) Correct the detector positions, accounting for the deflection of the scattered beam passing through the supermirror analyzer. The same deflection, corresponding to neutrons scattered elastically, is used for all scattered neutrons. This step is not needed for the unpolarized, or half-polarized (polarized incident beam, unpolarized scattered beam) measurements.
- (4) Correct the time of flight for the (incident-energy-dependent) moderator emission time.
- (5) Evaluate and subtract the time-independent background.

- (6) Convert events from time-of-flight to energy transfer.
- (7) Correct for the energy-dependent efficiency of the detectors.
- (8) Optionally, convert from the scattering cross-section to the dynamical structure factor.
- (9) Convert events from detector positions and energy transfer coordinates to momentum and energy transfer coordinates. Event data at this point is not on a regular grid.
- (10) Correct for spin flip efficiency [5] (polarized experiments only).
- (11) Histogram data onto a regular grid in reciprocal space.
- (12) Combine data from multiple measurements and/or multiple detectors, correctly accounting for the statistical weights
- (13) Correct for the energy dependent polarizer transmission.

If needed, the data can be histogrammed in energy prior to step 9 in order to obtain/save a histogram in energy transfer for each detector (typically, as a SPE/NXSPE file). Several programs [6, 7] use this format to perform the next steps for the unpolarized measurement.

Flipping ratio might be dependent on the sample orientation (like in the case of superconducting samples), so for statistical reasons we must perform this step before histogramming. The energy dependent polarizer transmission could in principle be performed at the same step, but some users would prefer the option of looking at the data without this correction.

4. Conclusions

This paper describes the challenges of data processing for polarized neutron experiments at the HYSPEC spectrometer, and the algorithms that we have developed to meet these challenges. Different hardware elements of the polarized setup were characterized, and the effects were considered in the data reduction workflow. Data output of the proposed workflow will be separated into different components (nuclear, magnetic, etc.) [8, 9]. Several tasks remain to be performed, such as accounting for the energy-dependent beam deflection by the supermirror analyzer, or understanding its effect on the resolution of the instrument.

This work was supported in part by the Paul Scherrer Institut by loaning the supermirror analyzer to Oak Ridge National Laboratory.

References

- [1] Winn B, Filges U, Garlea V O, Graves-Brook M, Hagen M, Jiang C, Kenzelmann M, Passell L, Shapiro S M, Tong X and Zaliznyak I 2015 *EPJ Web of Conferences* **83** 03017 URL <http://dx.doi.org/10.1051/epjconf/20158303017>
- [2] Arnold O, Bilheux J, Borreguero J, Buts A, Campbell S, Chapon L, Doucet M, Draper N, Leal R F, Gigg M, Lynch V, Markvardsen A, Mikkelsen D, Mikkelsen R, Miller R, Palmen K, Parker P, Passos G, Perring T, Peterson P, Ren S, Reuter M, Savici A, Taylor J, Taylor R, Tolchenov R, Zhou W and Zikovsky J 2014 *Nuclear Instruments and Methods in Physics Research Section A: Accelerators, Spectrometers, Detectors and Associated Equipment* **764** 156 – 166 ISSN 0168-9002 URL <http://dx.doi.org/10.1016/j.nima.2014.07.029>
- [3] Moon R M, Riste T and Koehler W C 1969 *Phys. Rev.* **181**(2) 920–931 URL <http://link.aps.org/doi/10.1103/PhysRev.181.920>
- [4] Zaliznyak I A, Savici A T, Garlea V O, Winn B, Filges U, Schneeloch J, Tranquada J M, Gu G, Wang A and Petrovic C 2017 *EPJ Web of Conferences* Unpublished, this PNCMI conference proceedings URL <https://arxiv.org/pdf/1610.06018v3.pdf>

- [5] Stewart J R, Deen P P, Andersen K H, Schober H, Barthélémy J F, Hillier J M, Murani A P, Hayes T and Lindenau B 2009 *Journal of Applied Crystallography* **42** 69–84 URL <http://dx.doi.org/10.1107/S0021889808039162>
- [6] Azuah R, Kneller L, Qiu Y, Tregenna-Piggott P, Brown C, Copley J and Dimeo R 2009 *J. Res. Natl. Inst. Stand. Technol.* **114** 341
- [7] Ewings R A, Buts A, Le M D, van Duijn J, Bustinduy I and Perring T G 2016 *Nuclear Instruments and Methods in Physics Research Section A: Accelerators, Spectrometers, Detectors and Associated Equipment* **834** 132 – 142 ISSN 0168-9002 URL <http://www.sciencedirect.com/science/article/pii/S016890021630777X>
- [8] Schärpf O and Capellmann H 1993 *physica status solidi (a)* **135** 359–379 ISSN 1521-396X URL <http://dx.doi.org/10.1002/pssa.2211350204>
- [9] Ehlers G, Stewart J R, Wildes A R, Deen P P and Andersen K H 2013 *Review of Scientific Instruments* **84** 093901 URL <http://scitation.aip.org/content/aip/journal/rsi/84/9/10.1063/1.4819739>